Electronic Supplementary Material for

A cations-modified cluster model for the density-functional theory simulation of potential dependent Raman scattering from surface complex/electrode systems

Song-Yuan Ding,[a,b] **Bi-Ju Liu,**[a] **Qing-Ning Jiang,**[a] **De-Yin Wu,**[a] **Bin Ren,**[a] **Xin Xu,**[a] **and Zhong-Qun Tian*[a]**

[a] *State Key Laboratory of Physical Chemistry of Solid Surfaces, and Department of Chemistry, College of Chemistry and Chemical Engineering, Xiamen University, Xiamen, China. Fax: +86-592-2181906; Tel: +86-592-2186979; E-mail: zqtian@xmu.edu.cn*
[b] *Theoretical Chemistry, Vrije Universiteit Amsterdam, De Boelelaan 1083, 1081 HV Amsterdam, The Netherlands.*

Computational Details and Experimental Conditions

Geometry optimization and vibrational frequencies for all pyridine complexes in this work were performed at the level of hybrid density functional B3LYP.[1, 2] All geometries were fully optimized, except for $(PyAg_4Cl_3Ag_{16}M_3)^0$ series. In $(PyAg_4Cl_3Ag_{16}M_3)^0$ series, we firstly pre-optimized $Ag_4Cl_3Ag_{16}M_3$ with C_{3v} symmetry with a lower convergence criteria of the geometric optimization in Gausian09, then added the pyridine attached on the top silver atoms of Ag_4, and made the lowermost Ag_6 layer and M_3 layer frozen during the further optimization with standard geometric convergence criteria.

In the calculation of the interaction energies between pyridine and the left substrate $Ag_4Cl_3Ag_{16}M_3$ of the super-Surface complexes (super-SCs) of $(PyAg_4Cl_3Ag_{16}M_3)^0$, we divided the super-SCs into pyridine and the left $Ag_4Cl_3Ag_{16}M_3$ fragment which we denoted S. Not only pyridine but also the $Ag_4Cl_3Ag_{16}M_3$ fragment is not re-optimized.

The basis sets 6-311++G** for H, C, N, O, Cl atom and LANL2DZ for Ag were utilized.[3] The reliability of method/basis sets has been well checked and used to study the chemical enhancement in pyridine/silver systems by many groups.[4, 5] Vibrational frequencies, normal modes and Raman activities were all calculated with the analytical method. The scale factor for the frequencies below 2000 cm^{-1} is 0.981, and that above 3000 cm^{-1} is 0.968. Frequency-dependent polarizability derivatives was calculated by coupled perturbed Hartree-Fock like (CPHF) method.[6] The vertical excitation energy and the corresponding oscillator strength were calculated with time-dependent density functional theory (TDDFT).[7] All calculations presented above were performed by using the Gaussian 09 package.[8]

On the basis of the optimized geometries, the static/dynamic Raman scattering factor S_i can be directly obtained from Gaussian output file, and then absolute Raman intensities (Stokes scattering) with the general formula in harmonic approximation, were estimated by the differential Raman scattering cross section (DRSC) given by,[9]

$$\left(\frac{d\sigma}{d\Omega}\right)_i = (2\pi)^4 \cdot \frac{h}{8\pi^2 c\tilde{v}_i} \cdot \frac{(\tilde{v}_0 - \tilde{v}_i)^4}{1 - \exp(-hc\tilde{v}_i / k_B T)} \cdot \frac{S_i}{45} \quad (S1)$$

where v_0 and v_i are the frequencies (in cm^{-1}) of incident light and i^{th} vibrational mode, respectively. S_i is the static/dynamic Raman scattering factor (in Å^4/amu) with respect to the ith vibrational mode, where static means static field perturbation corresponding to normal Raman spectrum (NRS), while dynamics means the time-harmonic field perturbation corresponding to frequency-dependent Raman

spectrum (FDRS). For each wavenumber, we sum over all contributions from the Lorenzian broaden of the DRSC for each peak.

Normally, if the static polarizability of the molecule in the equilibrium geometry is very large, the static polarizability with respect to the total symmetric normal mode is also very much. The absolute intensity of the simulated static Raman of the total symmetric normal modes can be understood in terms of the second order perturbation theory.[10]

The static polarizability can be expressed as,[10]

$$\alpha_{\alpha\beta} = -4 \sum_{i}^{occ} \sum_{m}^{vir} n_i P_{im}^{\alpha} T_{mi}^{\beta} \qquad (S2),$$

where n_i is the occupation number of the ith occupied orbital, index i and m run over all occupied orbital ϕ_i and virtual orbitals ϕ_m, respectively. The induced density matrix P_{im}^{α} by the perturbing dipole field in the α direction is,

$$P_{im}^{\alpha} = \frac{1}{\varepsilon_i - \varepsilon_m} \int d^3 r' \phi_i(r') \phi_m(r') \left[\delta v_{ext}(r') + v_{ind}^{\alpha}(r') \right] \qquad (S3),$$

where $\delta v_{ext}(r)$ is the external potential and $v_{ind}^{\alpha}(r')$ is the induced potential which includes the Coulomb potential and the exchange-correlation potential, and T_{mi}^{β} is the transition dipole matrix in β direction

$$T_{mi}^{\beta} = \int d^3 r' \phi_i(r) \mu^{\beta} \phi_m(r) \qquad (S4)$$

It can be easily seen that, the energy gap between the transition-allowed occupied − virtual molecular orbitals pair is smaller, and then the contribution to the total polarizability will be larger. It should be noted that, the aforementioned eqs. S2-S4

only work for static polarizability, for frequency-dependent Raman tensors, a frequency-dependent version, i.e., the time-dependent Kohm-Sham equations should be involved.

Experimentally, we used the cyclic linear potential method to sweep twice at 100 mV s^{-1} between 0 and + 900 mV relative to saturated calomel potential to roughen the silver electrode in KCl solution (pH = 2), so that the electrode was covered with AgCl layers. Then we immersed the electrode in 0.5 M KCl + 0.1 M pyridine solution and for experiment. The electrochemical Raman experiments were performed on a LabRam I system. The excitation line is 632.8 nm with power of 1.1 mW.
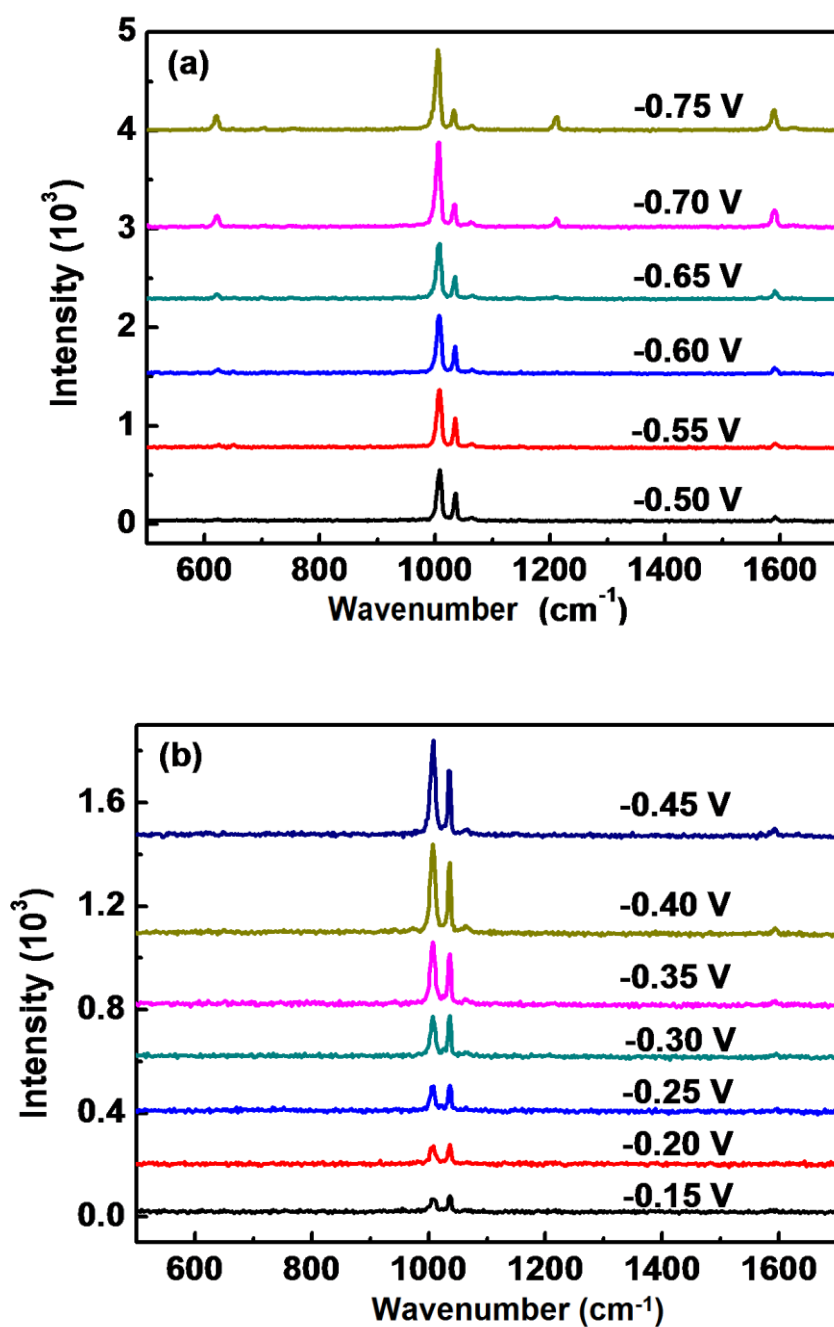
Fig. S1 Experimental surface Raman spectra of a roughened silver electrode in 0.5 M KCl + 0.1 M, with the applied potential from -0.75 to -0.50 V (a) and from -0.45 to -0.15 V (b), the excitation line: 632.8 nm.
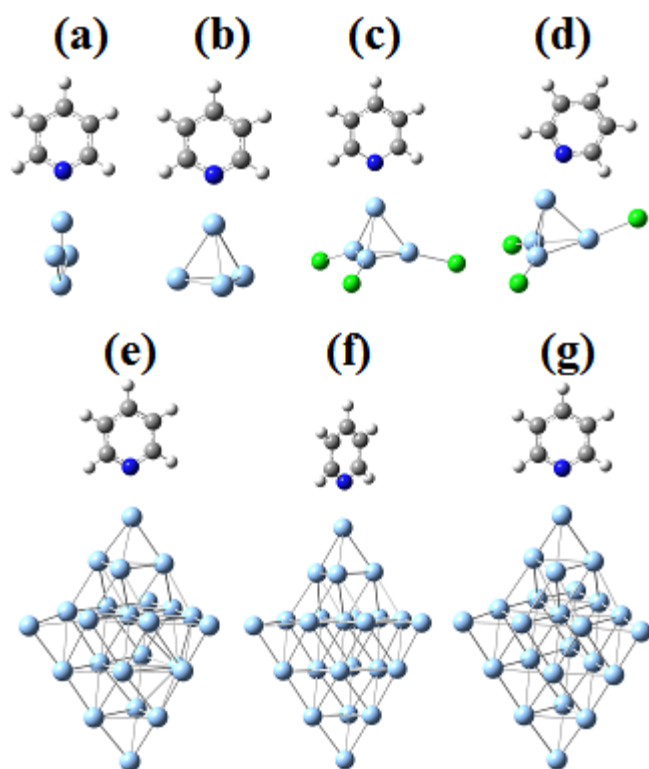
Fig. S2 The optimized geometries of (a) $PyAg_4^+$, (b) $PyAg_4^{2+}$, (c) $PyAg_4Cl_3^{2-}$, (d) $PyAg_4Cl_3^-$, (e) $PyAg_4Ag_{20}$, (f) $PyAg_4Ag_{20}^+$ and (g) $PyAg_4Ag_{20}^{2+}$.
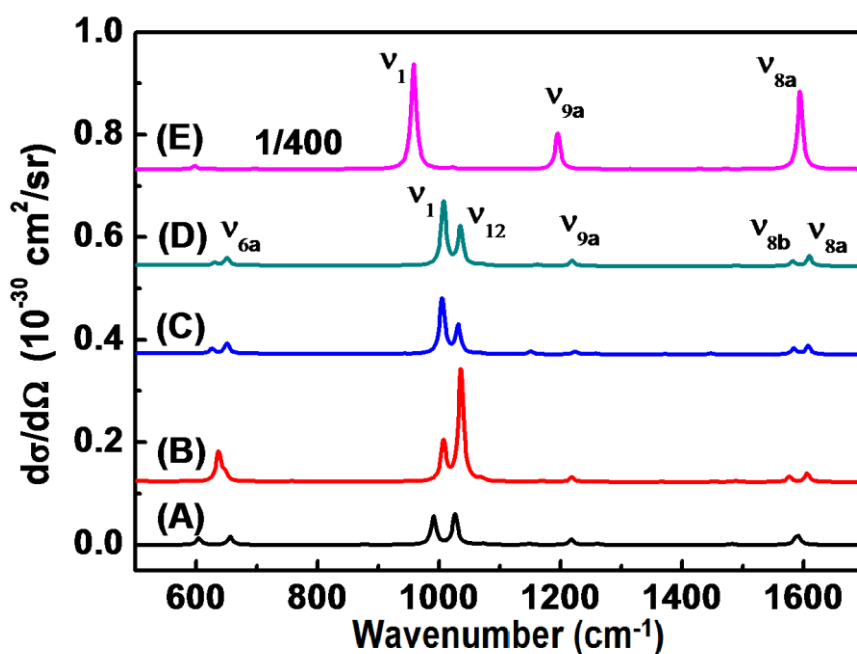
Fig. S3 Simulated normal Raman spectra (NRS) of free pyridine (Py) (A), and surface complexes (SCs), (B) $(PyAg_4)^+$, (C) $(PyAg_4)^{2+}$, (D) $(PyAg_4Cl_3)-$, and (E) $(PyAg_4Cl_3)^{2-}$, at an incident wavelength of 632.8 nm, differential cross section in units 10^{-30} cm^2/sr and Raman shift in cm^{-1}. Spectra have been broadened by a Lorenzian line shape with a width of 10 cm^{-1}.
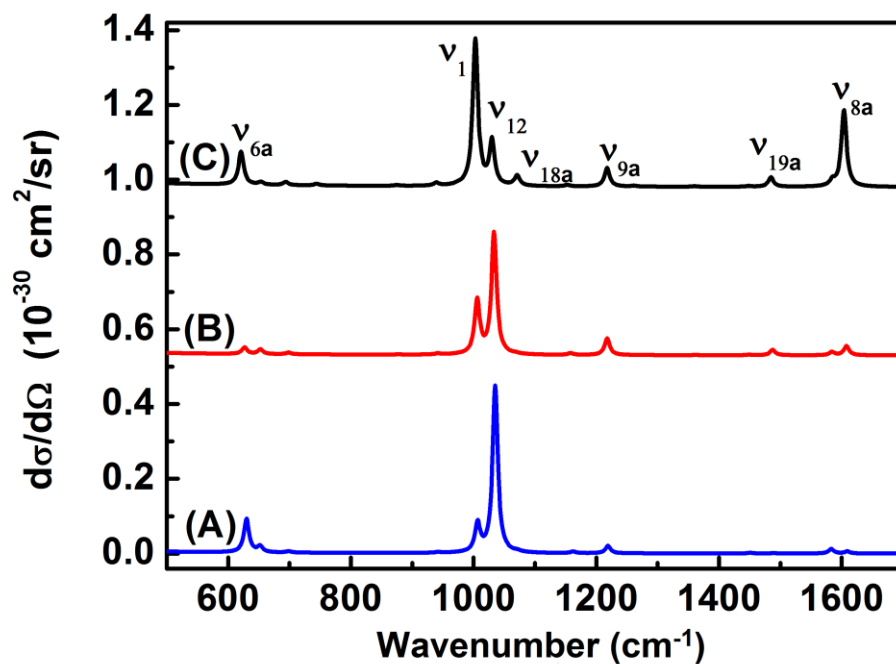
Fig. S4 Simulated normal Raman spectra of surface complexes (SCs) $(PyAg_4Ag_{20})^q$ $(q = 0, +1, +2)$ [(A) $(PyAg_4Ag_{20})^0$, (B) $(PyAg_4Ag_{20})^+$, and (C) $(PyAg_4Ag_{20})^{2+}$] at an incident wavelength of 632.8 nm, different cross section in units 10^{-30} cm^2/sr and Raman shift in cm^{-1}. Spectra have been broadened by a Lorenzian having a width of 10 cm^{-1}.
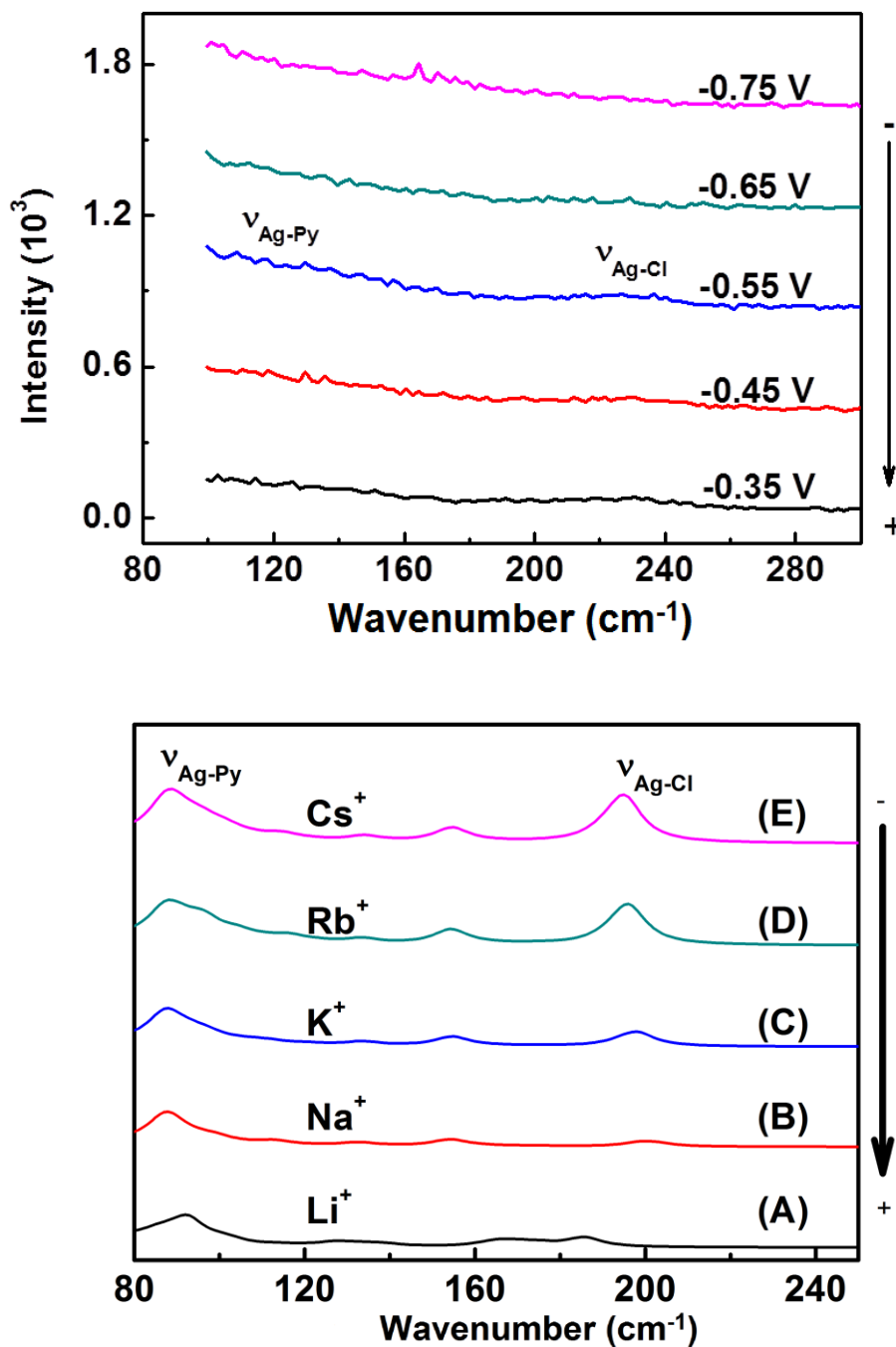
Fig. S5 (A) Experimental surface Raman spectra (a) to (e) of a roughened silver electrode in 0.5 M KCl + 0.1 M pyridine, at − 0.35, − 0.45, − 0.55, − 0.65 and − 0.75 V, respectively. The excitation line: 632.8 nm. (B) Simulated NRS (a) to (e) of SCs $(PyAg_4Cl_3)^0$ on the model surface with different "applied potential", $(Ag_{16}M_3)^{3+}$ ($M^+ = Li^+$, Na^+, K^+, Rb^+, Cs^+) at an incident wavelength of 632.8 nm, differential cross section in units 10^{-30} cm^2/sr and Raman shift in cm^{-1}. Spectra have been broadened by a Lorenzian line shape with a width of 10 cm^{-1}.
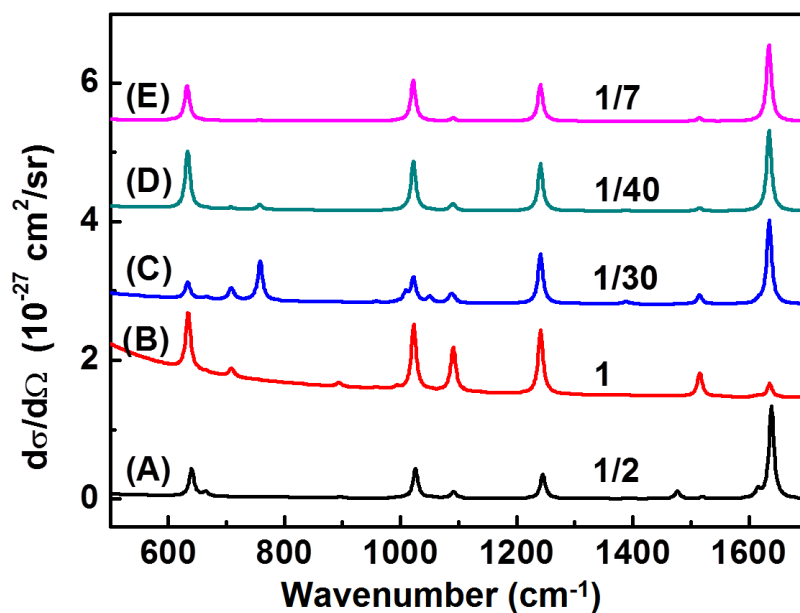
Fig. S6 Simulated frequency-dependent Raman spectra of (A) to (E) of super-SCs $(PyAg4Cl_3Ag_{16}M_3)^0$ (M^+ = Li^+, Na^+, K^+, Rb^+, Cs^+) (calculated by Coupled-Perturbation Hartree-Fock like method) with perturbing electric dipole field at the wavelength of 632.8 nm, differential cross section in units 10^{-27} cm^2/sr and Raman shift in cm^{-1}. Spectra have been broadened by a Lorenzian line shape with a width of 10 cm^{-1}.

The total symmetric vibrational modes (ν_{6a}, ν_1, ν_{12}, ν_{18a}, ν_{19a}, ν_{19a}, ν_{8a}) of pyridine

(using Wilson's notation for benzene[11]) of the structures considered in this work are

plotted in Fig S7.
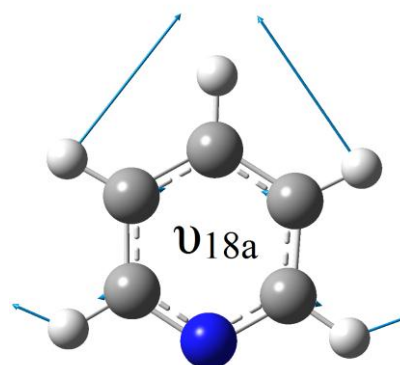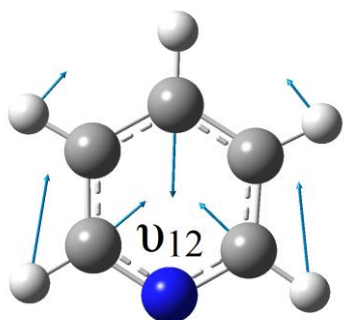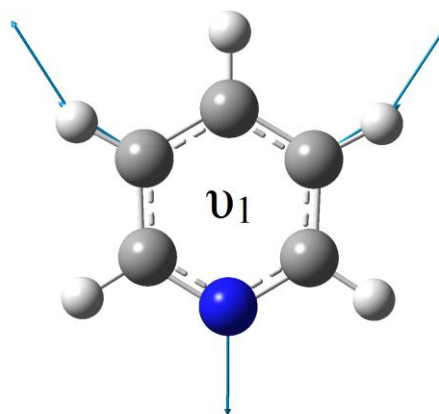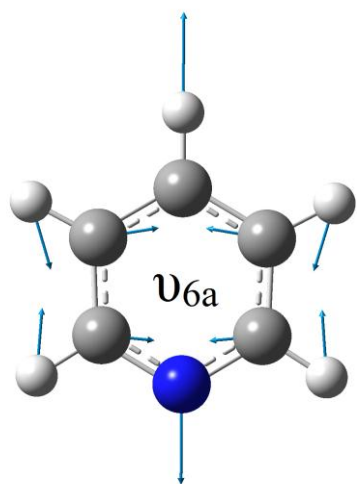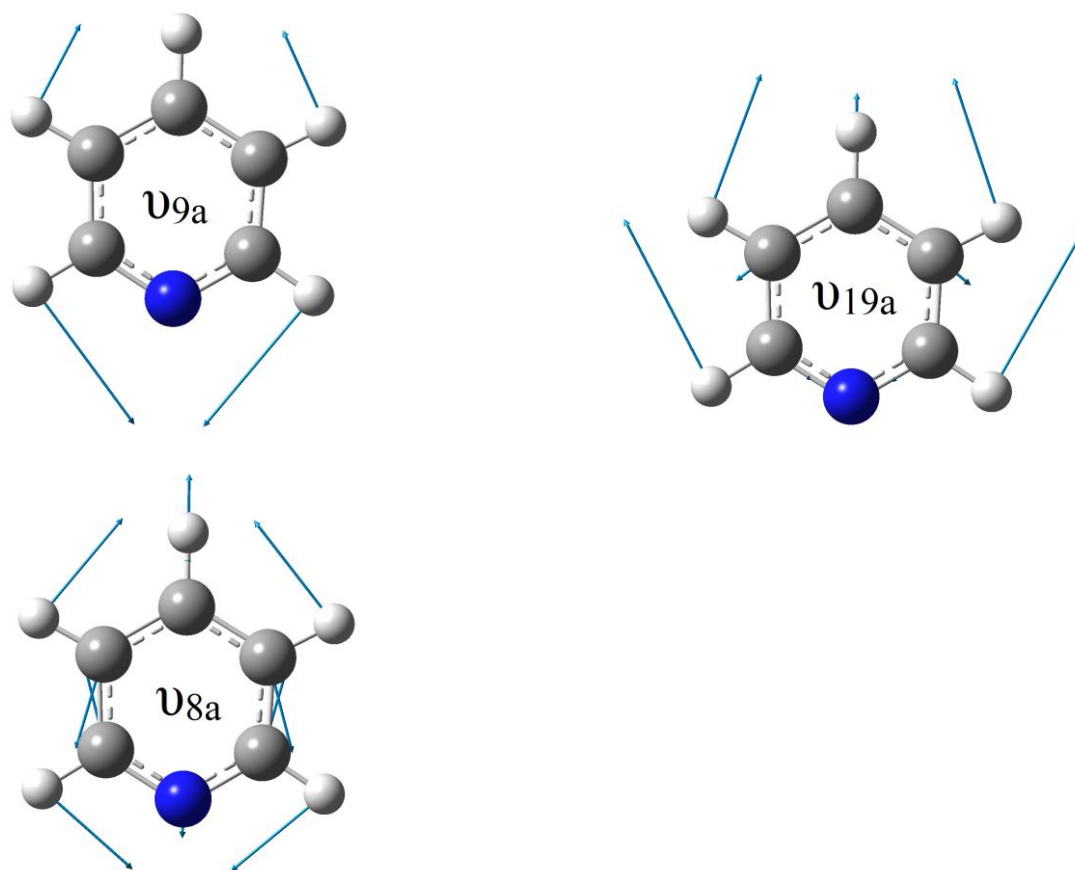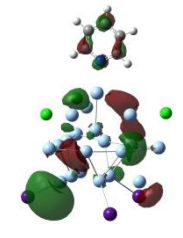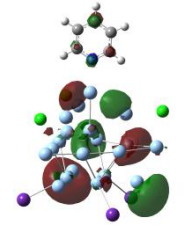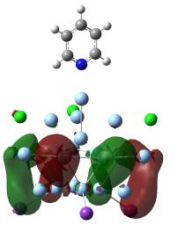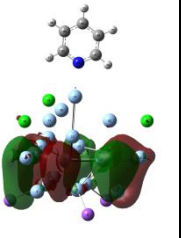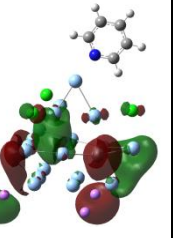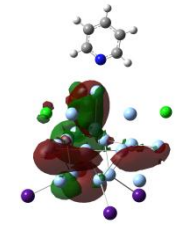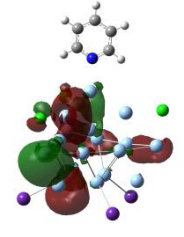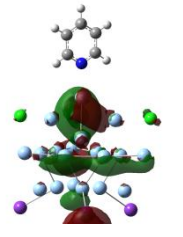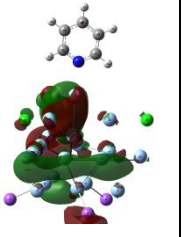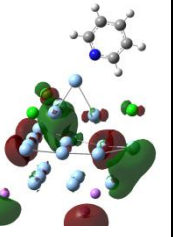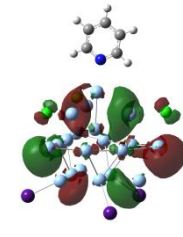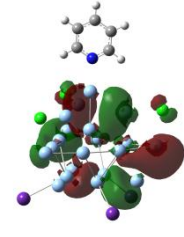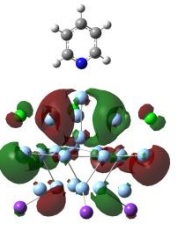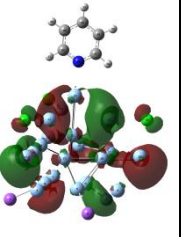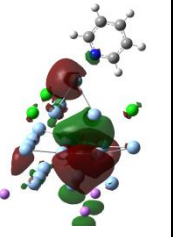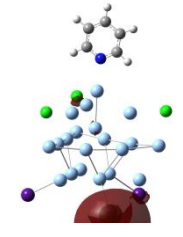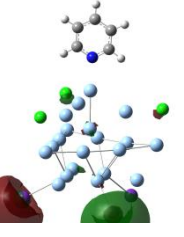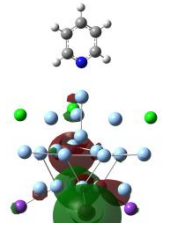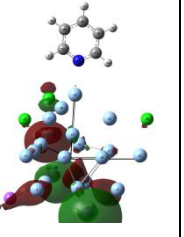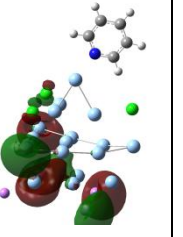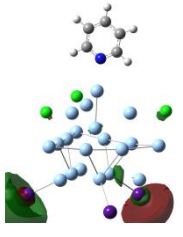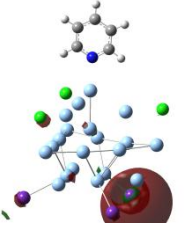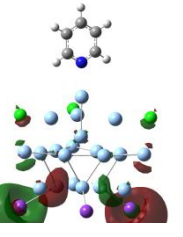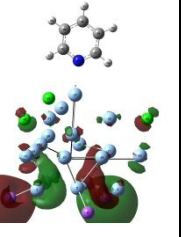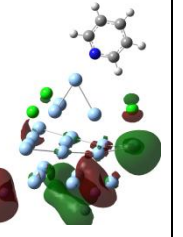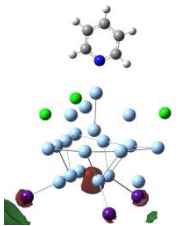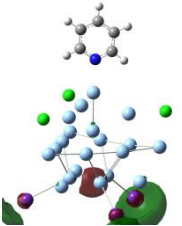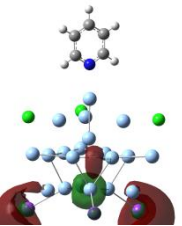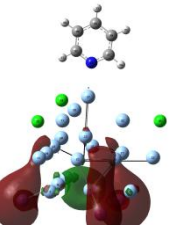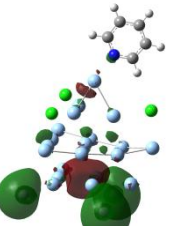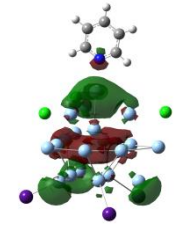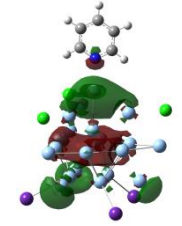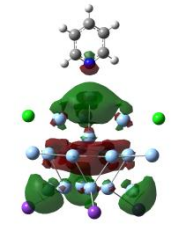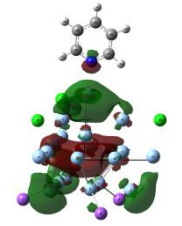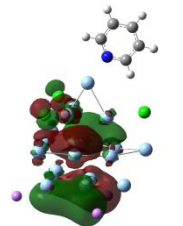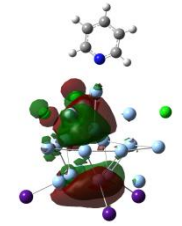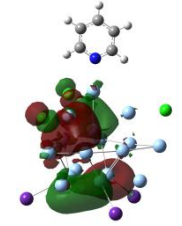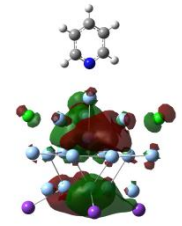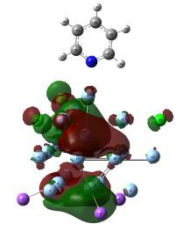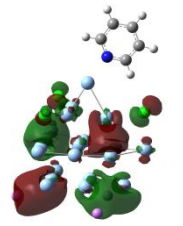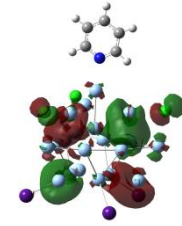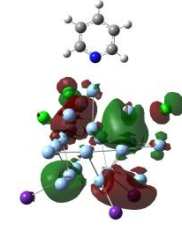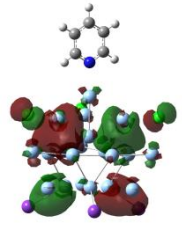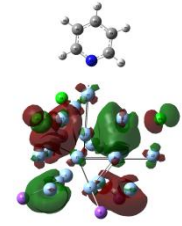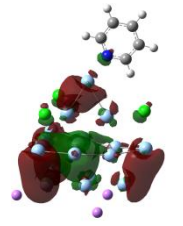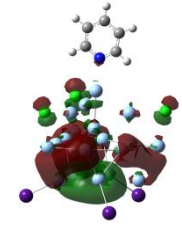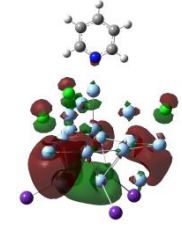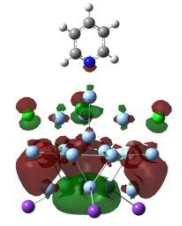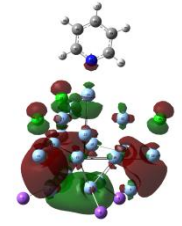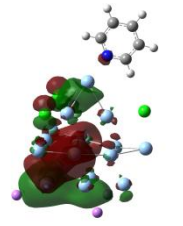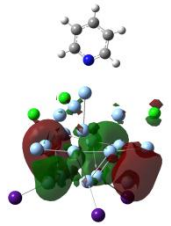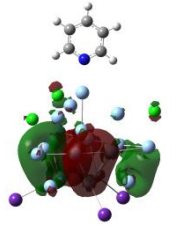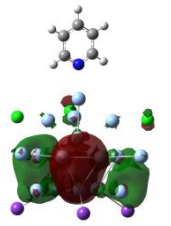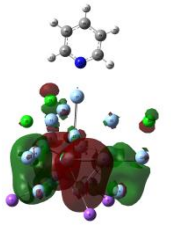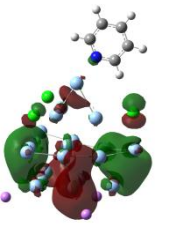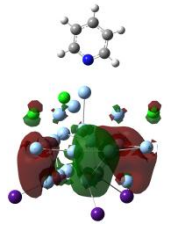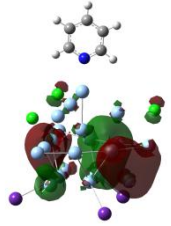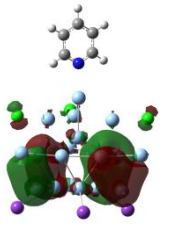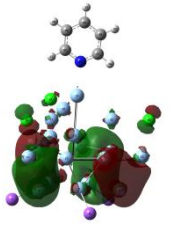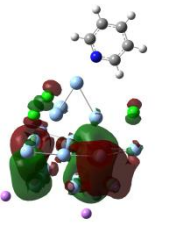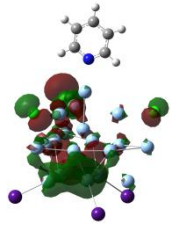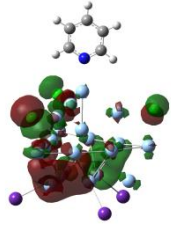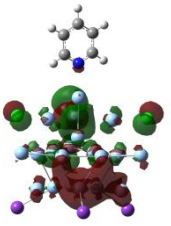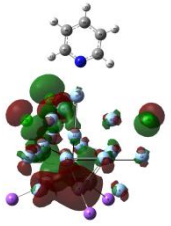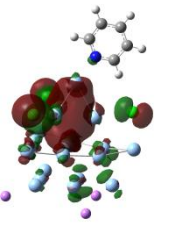
Fig. S7 The normal modes of υ_{6a}, υ_1, υ_{12}, υ_{6a}, υ_{8a}, υ_{9a}, υ_{19a} and υ_{8a} of pyridine.

Table S1 Selected molecular orbital plots of $(PyAg_4Cl_3Ag_{16}M_3)^0$ (where S= $Ag_4Cl_3Ag_{16}$, $M^+=Li^+$, Na^+, K^+, Rb^+, Cs^+), and the relative orbital energy with respective to the corresponding orbital energy of HOMO

	(Py-SCs$_3$)	(Py-SRb$_3$)	(Py-SK$_3$)	(Py-SNa$_3$)	(Py-SLi$_3$)
LUMO+9	2.496 eV	2.539 eV	2.587 eV	2.745 eV	2.479 eV
LUMO+8	2.423 eV	2.446 eV	2.418 eV	2.547 eV	2.388 eV
LUMO+7	2.413 eV	2.430 eV	2.400 eV	2.527 eV	2.353 eV
LUMO+6	2.349 eV	2.384 eV	2.392 eV	2.518 eV	2.187 eV

LUMO+5	2.330 eV	2.369 eV	2.364 eV	2.456 eV	2.128 eV
LUMO+4	1.972 eV	1.994 eV	1.999 eV	2.056 eV	2.119 eV
LUMO+3	1.957 eV	1.980 eV	1.969 eV	2.030 eV	2.015 eV
LUMO+2	1.736 eV	1.663 eV	1.877 eV	1.931 eV	1.651 eV
LUMO+1	1.719 eV	1.642 eV	1.840 eV	1.869 eV	1.629 eV

LUMO	1.624 eV	1.544 eV	1.727 eV	1.677 eV	1.419 eV
HOMO	0 eV	0 eV	0 eV	0 eV	0 eV
HOMO-1	-0.051 eV	-0.056 eV	-0.106 eV	-0.122 eV	-0.078 eV
HOMO-2	-0.081 eV	-0.082 eV	-0.147 eV	-0.158 eV	-0.518 eV
HOMO-3	-0.469 eV	-0.451 eV	-0.443 eV	-0.416 eV	-0.701 eV

HOMO-4	-0.512 eV	-0.507 eV	-0.582 eV	-0.596 eV	-0.756 eV
HOMO-5	-0.533 eV	-0.526 eV	-0.591 eV	-0.607 eV	-0.767 eV
HOMO-6	-2.141 eV	-2.133 eV	-2.170 eV	-2.160 eV	-2.207 eV

References

1. C. Lee, W. Yang and R. G. Parr, *Phys. Rev. B*, 1988, **37**, 785.
2. A. D. Becke, *J. Chem. Phys.*, 1993, **98**, 5648.
3. P. J. Hay and W. R. Wadt, *J. Chem. Phys.*, 1985, **82**, 270.
4. A. Vivoni, R. L. Birke, R. Foucault and J. R. Lombardi, *J. Phys. Chem. B*, 2003, **107**, 5547.
5. D. Y. Wu, M. Hayashi, Y. J. Shiu, K. K. Liang, C. H. Chang, Y. L. Yeh and S. H. Lin, *J. Phys. Chem. A*, 2003, **107**, 9658.
6. P. Pulay, *J. Chem. Phys.*, 1983, **78**, 5043.
7. M. E. Casida, C. Jamorski, K. C. Casida and D. R. Salahub, *J. Chem. Phys.*, 1998, **108**, 4439.

8.   M. J. T. Frisch, G. W.; Schlegel, H. B.; Scuseria, G. E.; Robb, M. A.; Cheeseman, J. R.; Scalmani, G.; Barone, V.; Mennucci, B.; Petersson, G. A.; Nakatsuji, H.; Caricato, M.; Li, X.; Hratchian, H. P.; Izmaylov, A. F.; Bloino, J.; Zheng, G.; Sonnenberg, J. L.; Hada, M.; Ehara, M.; Toyota, K.; Fukuda, R.; Hasegawa, J.; Ishida, M.; Nakajima, T.; Honda, Y.; Kitao, O.; Nakai, H.; Vreven, T.; Montgomery, Jr., J. A.; Peralta, J. E.; Ogliaro, F.; Bearpark, M.; Heyd, J. J.; Brothers, E.; Kudin, K. N.; Staroverov, V. N.; Kobayashi, R.; Normand, J.; Raghavachari, K.; Rendell, A.; Burant, J. C.; Iyengar, S. S.; Tomasi, J.; Cossi, M.; Rega, N.; Millam, N. J.; Klene, M.; Knox, J. E.; Cross, J. B.; Bakken, V.; Adamo, C.; Jaramillo, J.; Gomperts, R.; Stratmann, R. E.; Yazyev, O.; Austin, A. J.; Cammi, R.; Pomelli, C.; Ochterski, J. W.; Martin, R. L.; Morokuma, K.; Zakrzewski, V. G.; Voth, G. A.; Salvador, P.; Dannenberg, J. J.; Dapprich, S.; Daniels, A. D.; Farkas, Ö.; Foresman, J. B.; Ortiz, J. V.; Cioslowski, J.; Fox, D. J. , Gaussian, Inc., Wallingford CT, 2009.

9.   D. A. Long, *The Raman Effect: A Unified Treatment of the Theory of Raman Scattering By Molecules*, Wiley, 2002.

10. S. J. A. van Gisbergen, Vrije Amsterdam, 1998.

11. E. B. Wilson, *Phys. Rev.*, 1934, **45**, 706.